



Review

Hydrogen Containing Nanofluids in the Spark Engine's Cylinder Head Cooling System

Alexander Balitskii ^{1,2,*}, Myroslav Kindrachuk ³, Dmytro Volchenko ⁴, Karol F. Abramek ² , Olexiy Balitskii ⁵, Vasyly Skrypnyk ⁴, Dmytro Zhuravlev ⁴, Iryna Bekish ⁴, Mykola Ostashuk ⁶ and Valerii Kolesnikov ^{1,7} 

- ¹ Department of Strength of the Materials and Structures in Hydrogen-Containing Environments, Karpenko Physico-Mechanical Institute, National Academy of Sciences of Ukraine, 79-601 Lviv, Ukraine; kolesnikov197612@gmail.com
 - ² Department of Mechanical Engineering and Mechatronics, West Pomeranian University of Technology in Szczecin, 70-310 Szczecin, Poland; karol.abramek@zut.edu.pl
 - ³ Aerospace Faculty, National Aviation University, 03-058 Kyiv, Ukraine; nau12@ukr.net
 - ⁴ Institute of Mechanical Engineering, Ivano-Frankivsk National Technical University of Oil and Gas, 76-000 Ivano-Frankivsk, Ukraine; vol21@ukr.net (D.V.); skripnik-vs07@ukr.net (V.S.); dmytro.2103@ukr.net (D.Z.); Iryna.bekish@nung.edu.ua (I.B.)
 - ⁵ Department of System Design, Lviv Ivan Franko National University, 79-005 Lviv, Ukraine; olexiybal@yahoo.com
 - ⁶ Department of Transport Technologies, Lviv Polytechnic National University, 79-000 Lviv, Ukraine; mikola.ostashuk.M@gmail.com
 - ⁷ Department of Production Technology and Professional Education, Taras Shevchenko National University of Lugansk, 92-703 Starobilsk, Ukraine
- * Correspondence: balitski@ipm.lviv.ua



Citation: Balitskii, A.; Kindrachuk, M.; Volchenko, D.; Abramek, K.F.; Balitskii, O.; Skrypnyk, V.; Zhuravlev, D.; Bekish, I.; Ostashuk, M.; Kolesnikov, V. Hydrogen Containing Nanofluids in the Spark Engine's Cylinder Head Cooling System. *Energies* **2022**, *15*, 59. <https://doi.org/10.3390/en15010059>

Academic Editor: Flavio Caresana

Received: 30 October 2021

Accepted: 16 December 2021

Published: 22 December 2021

Publisher's Note: MDPI stays neutral with regard to jurisdictional claims in published maps and institutional affiliations.



Copyright: © 2021 by the authors. Licensee MDPI, Basel, Switzerland. This article is an open access article distributed under the terms and conditions of the Creative Commons Attribution (CC BY) license (<https://creativecommons.org/licenses/by/4.0/>).

Abstract: The article is devoted to the following issues: boiling of fluid in the cooling jacket of the engine cylinder head; agents that influenced the thermal conductivity coefficient of nanofluids; behavior of nanoparticles and devices with nanoparticles in the engine's cylinder head cooling system. The permissible temperature level of internal combustion engines is ensured by intensification of heat transfer in cooling systems due to the change of coolants with "light" and "heavy" nanoparticles. It was established that the introduction of "light" nanoparticles of aluminum oxide Al_2O_3 into the water in a mass concentration of 0.75% led to an increase in its thermal conductivity coefficient by 60% compared to the base fluid at a coolant temperature of 90 °C, which corresponds to the operating temperature of the engine cooling systems. At the indicated temperature, the base fluid has a thermal conductivity coefficient of $0.545 \frac{W}{(m^2 \times ^\circ C)}$, for nanofluid with Al_2O_3 particles its value was $0.872 \frac{W}{(m^2 \times ^\circ C)}$. At the same time, a positive change in the parameters of the nanofluid in the engine cooling system was noted: the average movement speed increased from 0.2 to 2.0 m/s; the average temperature is in the range of 60–90 °C; heat flux density 2×10^2 – $2 \times 10^6 \frac{W}{m^2}$; heat transfer coefficient 150–1000 $\frac{W}{(m^2 \times ^\circ C)}$. Growth of the thermal conductivity coefficient of the cooling nanofluid was achieved. This increase is determined by the change in the mass concentration of aluminum oxide nanoparticles in the base fluid. This will make it possible to create coolants with such thermophysical characteristics that are required to ensure intensive heat transfer in cooling systems of engines with various capacities.

Keywords: internal combustion engine; cylinder head; nanofluid; nanoparticles

1. Introduction

The problems of modern piston engine depend on increasing the power and motor resource of the engine; the qualitative composition of combustible mixtures and ensuring multilayeredness, taking into account toxicity and harmful emissions; starting systems (for diesel engines) and fuel injection; limiting mechanical and thermal tension. Currently, work is underway to improve the characteristics of internal combustion engines and their

systems: fuel supply, combustion, lubrication, air supply, and cooling. Therefore, for example, when assessing the heat balance of ship engines, the effective power interval varies from 31.0 to 41.8%, and the losses in the coolant are from 10.5 to 22.9%.

2. Literature Survey

Investigation and development of a methodology for assessing the structural elements' durability in hydrogen containing environment (moister air-cooled diesel engines cylinder heads, air-cooled with sea water admixture turbine blades, hydrogen-cooled generators retaining rings, cooled and lubricated systems by nano fluids and colloids with oxides, chalcogenide's nanoparticles, etc.) is actually due to wide application of the traditional and advanced technology with possible hydrogen saturation during long term service and engines hydrogen cleaning effect [1–64]. From the investigation of the operation principle of internal combustion engines [1,3–5,9,35–37], it follows that the mechanical movement of its elements is largely determined by the kinematics of the crank mechanism, fluid hydrodynamics in the channels, as well as more complex forms of movement: chemical and thermal movement, that is the processes of releasing and transferring the heat to the working fluid in the engine cylinder. Thermodynamic and heat transfer are important systems in the engine [6–10,13,18,21].

The nature of the processes taking place in this system has a decisive influence on the processes in the mechanical and hydraulic systems and, therefore, on the engine operation overall. Thermodynamics determines the amount of heat (Q), gas parameters (temperature, pressure, and specific volume), and specific heat flux (q). Heat transfer includes free and forced convective heat transfer, as well as conductive and radiative heat transfer. In this case, they operate mainly with the coefficients of thermal conductivity and heat transfer, forgetting about the heat transfer coefficient. Moreover, researchers [6–10,13,18,21] do not pay attention to the thermal resistance of heat transfer types and gas–liquid boundary layers.

The use of nanofluids containing nanometer-sized particles in cooling systems of motors, generators, braking devices, heating, and ventilation can increase growth the heat transfer coefficient due to a magnification in the thermal conductivity coefficient. The large scatter of experimental data is associated with a number of objective reasons: the method of oxides, intermetallides, chalcogenides nanoparticle synthesis, the “heavy” nanoparticle size distribution function [17,22,23,25], the nanofluid preparation technology [65–115], as well as the method for measuring thermal conductivity and interpreting the results. In order to use nanofluids as a coolant, it is necessary to have information of their thermophysical properties. For this goal, an analysis of papers that are dedicated to the study of nanofluids was carried out. Papers dedicated to the study of heat transfer in nanofluids [12–14] show that the thermal conductivity of arrest of ultrafine oxides “light” nanoparticles of aluminum, silicon, and titanium in water at a bulk concentration of several percent transcend the thermal conductivity of pure fluid by tens of percent [116].

The outcome of the experiment with nanoparticles of various sizes show that the thermal conductivity of a fluid based on larger particles is well declared using Maxwell's theory [13,18]. First of all, the data received were correlative with theoretical models which were cultivated to report the thermal conductivity and roughly dissipate suspensions. The first such model was constructed by Maxwell [13], who obtained the relation between the thermal conductivity λ of suspensions and the base fluid λ_0 . Analysis of the effect of the nanoparticles size on the thermal conductivity coefficient (α) shows the λ coefficient of nanofluids growth with a magnification of nanoparticles size [15]. The modeling of the thermal conductivity coefficient of a nanofluid is presented in [16] as a function of different nanoparticles' masses. The authors found out that λ at fixed sizes and concentrations of nanoparticles increases with a rise in their mass. The dependence of nanofluid's thermal conductivity coefficient on the mass of nanoparticles means the same dependability on the density of particles at the same size.

The thermal conductivity coefficient of nanofluids is also influenced by the shape of nanoparticles, which can be spherical, cylindrical, prismatic, flat, and elliptical. Thus,

in [13,14], the thermal conductivity of nanofluids with ZnO “heavy” nanoparticles having prismatically and spherical shapes was experimentally detected at different bulk concentrations of nanoparticles in the range from 0.05 to 5.0%. It was found that the λ coefficient of nanofluids with zinc oxide nanoparticles increased by 12.0% and 18.0%, respectively, for the globular and prismatically shapes of nanoparticles at $\varphi = 5.0\%$, compared to the λ coefficient of the base fluid—water. Nevertheless, many experimental data received to date have a wide scatter and often contradict each other. Some of the data indicate an anomalous increase in the thermal conductivity of nanofluids in comparison with theory [12]. Notwithstanding, in the course of joint research carried out by organizations from different countries, no anomalous increase in thermal conductivity at low concentrations of nanoparticles was found [17]. The classification of nanofluids and the analysis of theoretical advances to modeling the transfer coefficients are given in [19]. In particular, it is noted that a rigorous theory of transfer processes in nanofluids has not yet been developed, and the application of thermal conductivity modeling by molecular dynamics methods still gives predictions different from the classical theory [33–41]. However, none of the works mention how to avoid sediment on the bottom of the engine cooling channel of “light” nanoparticles under the action of inertial and gravitational forces. The main questions addressed in the article are the following: factors influencing the thermal conductivity coefficient of nanofluids (including very high value in pure hydrogen or hydrogen containing); boiling of liquid in the cooling jacket of the engine cylinder head; behavior of nanoparticles and devices with nanoparticles in the engine cylinder head cooling system; the discussion of the results [117–184], taking into account degradation of modern structural materials under the hydrogen containing environment influence [2,24,32,43–51,63,118,175,176].

3. Problem Formulation

Nanofluids can be used in heat exchange systems for cooling machines and units for various purposes: in disc-shoe brakes of hoisting machines, in self-ventilated disc-shoe brakes of vehicles, in tape-shoe brake pulleys of drawworks. In this case, hydrogen containing cooling systems with nanoparticles can be stationary and rotating. The purpose of this work is to substantiate the role of nanoparticles and their devices in increasing the thermal conductivity of a fluid in the internal combustion engine’s cooling system.

4. Fluid Boiling in the Cooling Jacket of the Engine Cylinder Head

Boiling is the thermal process of substance transition from a liquid to a gaseous phase, which occurs near a heated solid surface or in a layer of superheated liquid near the surface. The boundaries of the phase transition arise in the process of vaporization during boiling. Boiling can occur in a stationary and mobile liquid volume. The second option takes place in the cooling system of an internal combustion engine.

The bulk saturation temperature of the liquid T_s is taken as the reference point, considering the boiling of the liquid. Liquid below the saturation volume T_f is called underheated temperature. Underheating is indicated by $\Delta T_{Sub} = T_s - T_f$. In relation to the jacket’s wall overheating is the excess of the saturation temperature. The difference between the wall temperature T_w and the saturation temperature is called overheating and is denoted by $\Delta T_{Sub} = T_w - T_f$.

The boiling process of an underheated liquid in a channel with heat supply from the walls is characterized by a number of alternating modes as the heating increases. The regularities of changing the parameters of the heated liquid in the engine’s cooling system channel of the cylinder head are shown in modified Figure 1 [13].

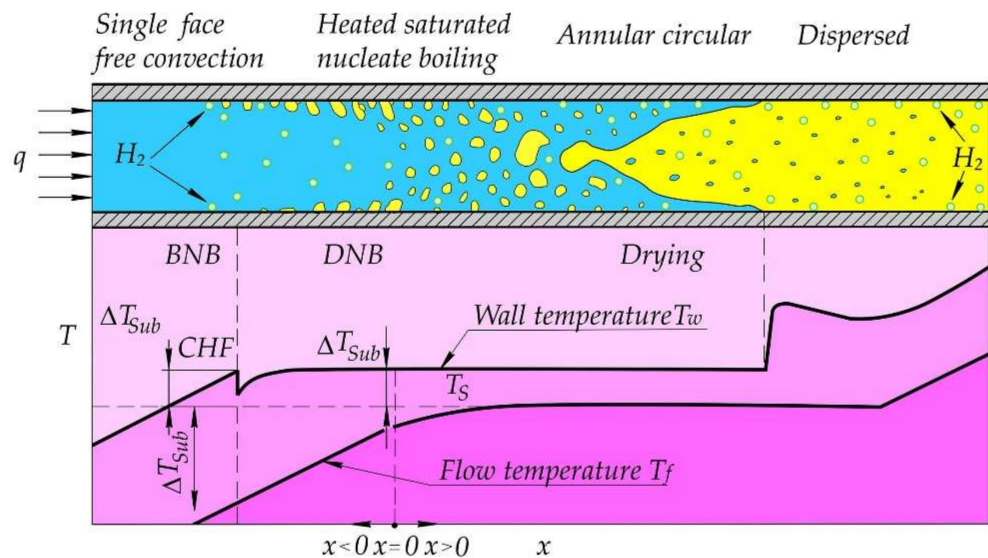


Figure 1. Regularities of the heated liquid parameters' changes in the channel of the engine's cylinder head cooling system: *BNB* and *DNB*—the beginning of nucleate boiling and its development; *CHF*—point of critical heat flow; x —mass steam quality [13].

The first segment on the graph is the single-phase free convection mode at nonsteaming conditions. As the bulk temperature of the wall rises above the saturation temperature of the liquid, vapor bubbles begin to form in microcavities and irregularities on the surface of the jacket wall. This point is called the beginning of nucleate boiling (hereinafter-*BNB*). At some distance from the *BNB*, bubbles are formed on the inner surface of the jacket. With heating increase, the bubbles grow in size and begin to detach from the wall. From this moment, the flow becomes two-phase. With further heating, the rate of growth and detachment of bubbles increases, and they merge into steam jets coming from the wall surface. This process is called developed (advanced) nucleate boiling (hereinafter *DNB*).

Heat transfer between *BNB* and *DNB* in this mode is mainly convective with an increasing input from boiling. With heat transfer constant increase at the *BNB* point, a decrease in the wall temperature occurs, due to the fact that part of the heat is spent on the transition phase. With an enlargement of the heat supply, convective heat transfer decreases, and by the time of the transition to the *DNB* it noticeably decreases.

Local heat exchangers with different shapes and masses provide intensive heat removal from different levels of the base fluid circulating in stationary and rotating equipment cooling systems. When removing Joule heat using a local heat exchanger in a branch of a thermoelectric cooler, the Peltier effect increases significantly. Local heat exchangers with different shapes and masses provide intensive heat removal from different levels of the base fluid circulating in stationary and rotating equipment cooling systems. When removing Joule heat using a local heat exchanger in a branch of a thermoelectric cooler, the Peltier effect increases significantly. The goal of enhanced heat transfer is to encourage or accommodate high heat fluxes. Cooling is one of the most important challenges facing engine performance. Due to limited space at the front of the engine, the size of the radiator is restricted and cannot be essentially increased. Therefore, it is necessary to increase the heat transfer capabilities of working fluids. With the advancement of nanotechnology, the new generation of heat transfer fluids called nanofluids have been developed and these fluids offer higher heat transfer properties compared to that of conventional automotive engine coolants [183]. One cooling technique that has demonstrated good performance in the cooling of electronics is the Peltier effect thermo electric cooler (*TEC*). The (*TEC*) is compact and provides a temperature differential below the ambient conditions without the need for moving parts or vapor compression plumbing [184].

The bubbles detached from the wall after the *BNB* have a hydrogen saturation temperature of the fluid, while the fluid itself is subcooled in the flow. In this case, vapor and liquid are in a nonequilibrium thermodynamic state. When the liquid reaches the saturation temperature, an equilibrium state of the two-phase flow is established, and the boiling mode is called saturated. The equilibrium state is characterized by the relative enthalpy of the flow x_b :

$$x_b = \frac{h_f - h'}{r} \quad (1)$$

here, h_f —specific enthalpy of the flow; h' —specific enthalpy of liquid in saturation state; r —specific heat of vaporization.

The relative enthalpy has a negative value at subcooled boiling and is equal to the mass vapor content x , that means it is in the range $0 \leq x \leq 1$ at the saturated state.

The boiling curve is the dependence of the heat flow through the wall on the wall temperature or the degree of wall overheating. An example of a boiling curve is shown in Figure 2. The first segment of the $A - B$ curve is a zone of free convective heat transfer, there is no boiling at this stage. Point B' corresponds to *BNB*. The transition from point B' to point B'' goes with the temperature drop which is associated with the consumption of heat, needed for the steam bubbles formation [16,101,104,108,137,139,143,145,150,157,159]. In the transient mode, the intensity of the process is influenced by various factors: the physical properties of the liquid and the material of the heating wall, the shape and orientation of the heating surface, its roughness, etc. This is followed by the area of partially developed nucleate boiling ($B'' - C$), which passes into the *DNB* ($C - D$). Point D in the nucleate boiling mode corresponds to the *CHF*. At this moment, an insulating vapor film begins to form on the inner surface of the wall, affecting heat exchange processes. A transition to film boiling occurs on the $D - E$ segment, and the $E - F$ segment corresponds to developed film boiling. The first crisis is characterized by the value q_{cr} , which depends mainly on the properties of the liquid, the density of its vapor, the acceleration of gravity, the shape and orientation of the heating surface. In addition to that, the conditions of wettability, roughness, and the material of the heating surface have a certain influence. The position of the second boiling crisis (q_{cg2} , ΔT_{cg2}) is determined by the same parameters as the first crisis. At the same time, there are two fundamental approaches to determining the position of the second crisis—hydrodynamic and thermodynamic. The part of the $D - E$ curve marked with dots denotes a sharp jump in the wall temperature after the *CHF*.

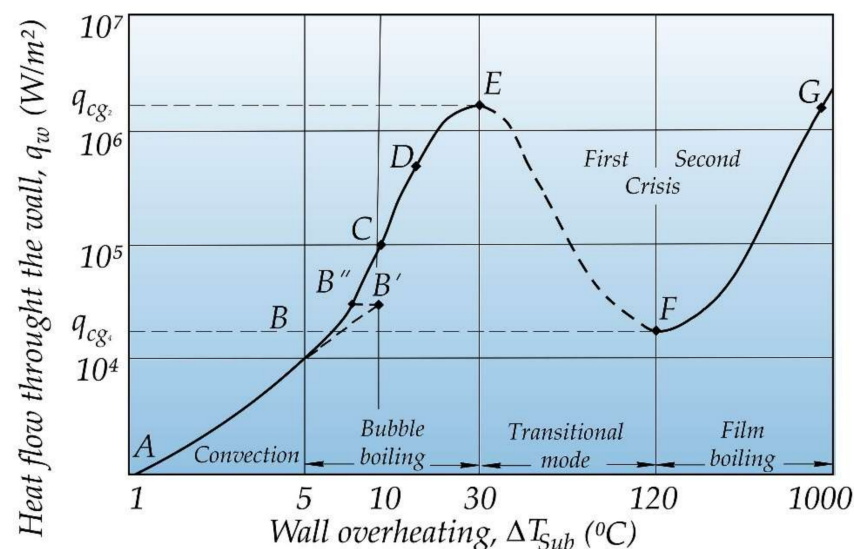


Figure 2. Regularities of modification in the heat flow penetrating the wall of cylinder head cooling jacket from the wall of its overheating.

With a heating increase the mode of developed nucleate boiling is replaced by slug, annular, and dispersed modes which are characterized by an increase in the volumetric vapor content. When the layer of liquid covering the wall evaporates, it dries up and that goes with a sharp decrease in the heat transfer coefficient, which leads to an increase in the bulk temperature of the wall. Heat fluxes corresponding to these modes are outside the range which is typical for engine cooling systems [60,82,124,160].

In addition to the drying mode, a decrease in heat transfer can also be observed with developed nucleate boiling and it is associated with the vapor layer formation caused by the accelerated growth of bubbles and its coalescence. Ultimately, the vapor film completely covers the surface, isolating it from the liquid. This mode is called film boiling. The point of transition to film boiling corresponds to the maximum heat flux and is called the point of critical heat flux (hereinafter *CHF*). It was established that the introduction of light nanoparticles of aluminum oxide Al_2O_3 into the water in a mass concentration of 0.75% led to an increase in its thermal conductivity coefficient by 60% compared to the base fluid at a coolant temperature of 90 °C, which corresponds to the operating temperature of the engine cooling systems. At the indicated temperature, the base fluid has a thermal conductivity coefficient of $0.545 \frac{W}{(m^2 \times ^\circ C)}$, for nanofluid with Al_2O_3 particles its value was $0.872 \frac{W}{(m^2 \times ^\circ C)}$. At the same time, a positive change in the parameters of the nanofluid in the engine cooling system was noted: the average movement speed has increased from 0.2 to $2.0 \frac{m}{s}$; the average temperature is in the range of 60–90 °C; heat flux density 2×10^2 – $2 \times 10^6 \frac{W}{m^2}$; heat transfer coefficient 150–1000 $\frac{W}{(m^2 \times ^\circ C)}$.

When there is a boiling in the cooling cavities, the calculation of heat transfer becomes more complicated. The phase action process affects both the heat transfer mechanism and the dynamics of the liquid flow [55,68,84,94,158].

5. Factors Affecting the Thermal Conductivity Coefficient of Nanofluids

In order to intensify heat transfer in cooling systems of heat engines, the possibility of using cooling nanofluids providing an increased coefficient of thermal conductivity has been recently considered [14]. Nanofluids have new properties that make them promising in the fields of heat transfer, tribology, etc. [15].

Nanofluids are persistent and stable two-phase suspensions “liquid–solid particles”. These solid particles are called nanoparticles, which have sizes up to 100 nm and provide a thermal conductivity coefficient many times higher than the thermal conductivity coefficient of the base coolant. Metals, oxides of metals, and non-metals, as well as materials based on carbon can be used as materials for nanoparticles. Base fluids can be used as liquids that allow to create cooling nanofluids which meet the main operational requirements and this happens when solid nanoparticles are added into liquids. The values of the thermal conductivity coefficients of nanoparticles of various materials are presented in Table 1.

Table 1. The values of thermal conductivity coefficient λ , $\frac{W}{(m \cdot K)}$ of nanoparticles of various materials at temperature 20 °C [14].

Material of nanoparticles	Thermal conductivity coefficient	λ , W/(m·K)
Aluminum, Al		237
Aluminum oxide, Al_2O_3		40
Cooper, Cu		401
Copper oxide, CuO		76.5
Carborundum, SiC		120
Aurum, Au		318
Carbon nanotubes		~3000
Graphene oxide		~3500
Graphene		~3000–5000

From the working efficiency point of view, nanofluids should be stable, resistant to agglomeration of solid nanoparticles and their precipitation during service life. It is

important to note that there should be no chemical reactions in nanofluids. From the operational point of view, when using nanofluids as a coolant for the engine cooling system, they should not cause corrosion of structural metals which are used in engine building, should not corrode non-metallic materials of seal systems, hoses, gaskets, etc.

The thermal conductivity coefficient of nanofluids is influenced by the following main factors: concentration of nanoparticles in the base fluid; nanofluid temperature; thermal conductivity coefficient of nanoparticles; size, shape and weight of nanoparticles; specific surface area of nanoparticles; technology of nanoparticles manufacturing; methods for dispersing nanoparticles in a base fluid; physical and mechanical properties of the base fluid.

An increase of nanoparticles concentration in base fluids, in the general case, provides an increase of nanofluid thermal conductivity (Figure 3) [13].

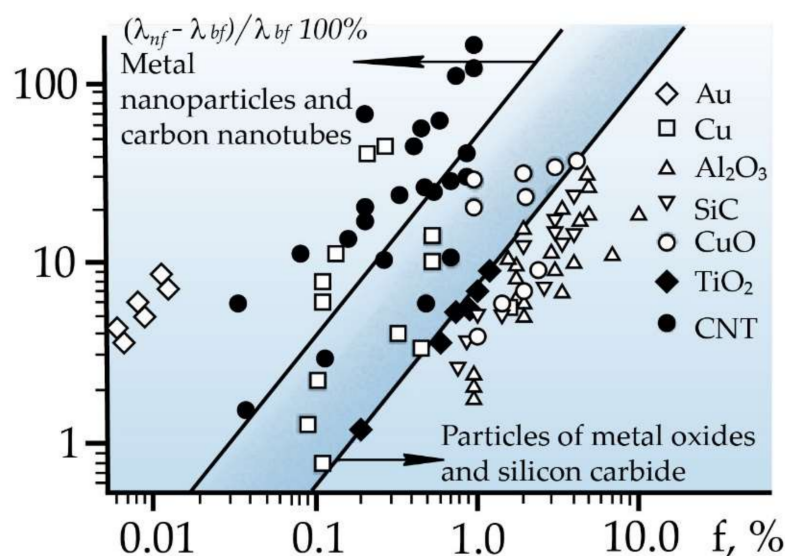


Figure 3. Dependence of the relative thermal conductivity coefficient of nanofluids on the volume concentration ($\phi, \%$) of various types of nanoparticles: λ_{nf} and λ_{bf} thermal conductivity coefficients of the nanofluid and the base fluid [16].

It should be noted that there is a general tendency towards a linear dependence of the thermal conductivity coefficient on the nanoparticles concentration. The nonlinear dependence of the thermal conductivity coefficient on the concentration of carbon nanotubes and nanoparticles having a spherical shape is presented in [13,14]. Nanofluids that are made based on nanoparticles with more thermally conductive materials show a greater increase in the λ coefficient compared to less thermally conductive materials.

The thermal conductivity coefficient of nanofluids with planar two-dimensional nanoparticles depends on the specific surface area of those particles, i.e., on the ratio of surface area of a particle in its mass (Table 2) [13].

Table 2. Thermal conductivity coefficient of nanofluids with flat nanoparticles depending on their specific surface area at various mass concentrations of nanoparticles in the base fluid (ϕ_m) [14].

$\phi_m, \%$ $s, m^2/g$	Thermal Conductivity Coefficient $\lambda, W/(m \cdot K)$			
	0.025	0.05	0.075	0.1
300	0.66	0.68	0.70	0.72
500	0.69	0.72	0.74	0.77
750	0.71	0.75	0.77	0.80

One of the perspective ways to control the value of nanofluids' thermal conductivity coefficient is the concentration of nanoparticles. The technology for producing nanoparticles and the method of their dispersion in base fluids determine many of the factors considered. Three methods of dispersion are best known: method 1—mechanical crushing of nanoparticles; method 2—the use of polymers wrapping around the nanoparticles; method 3—the usage of filtration of nanoparticles.

All three methods will be implemented further on.

All other conditions being equal, the technology of dispersing or nondispersing the same solid nanoparticles in different base fluids will affect the thermal conductivity of the nanofluid.

When creating nanofluids, it is necessary to select the base fluid, the material of nanoparticles and their shape, based on the energy load of the engine cylinder head.

6. Behavior of Nanoparticles in the Engine Cylinder Head Cooling System

Let us consider the types of nanofluids and their thermophysical parameters. The dynamic viscosity of a liquid is primarily defined by molecular interactions that limit the mobility of molecules. In a liquid, a molecule can penetrate into an adjacent layer only when a crack appears in it, sufficient for the molecule to penetrate it. The formation of cracks ("loosening" of the liquid) requires the activation energy of viscous friction. This energy decreases with temperature increase and pressure decrease. This is one of the reasons for the sharp decrease in the viscosity of the liquid with increasing temperature and its growth at high pressures.

The appearance in dispersed systems of spatial structures which are formed by macromolecules causes a sharp increase in viscosity. During the structured fluid flow, the work of the external force is spent not only on overcoming the true (Newtonian) viscosity, but also on the destruction of the structure. The viscosity of a liquid depends on the chemical structure of the molecules and increases with the increase of molecular weight. Studies have shown that nanofluids, starting with a certain concentration of nanoparticles in them, become non-Newtonian [12]. The considered water-based nanofluids with copper oxide (CuO) nanoparticles at their volume concentrations above 3.0% turn out to be viscoplastic, and their rheology is described by power functions for the liquid. The degree of rheology deviation of nanofluids from Newtonian values increases with an increase in these concentrations. The difficulty lies in the fact that the determination of the heat transfer coefficients is a complex task, since this requires the values of nanofluids' dynamic viscosity and their thermal conductivity coefficients.

The heat transfer coefficient of a nanofluid can be increased by varying the size of the particles, i.e., their interaction area with the liquid or by converting it into vapor. At the same time, an increase of particle size contributes to a decrease of heat transfer coefficients. In addition, during heat transfer in systems with nanofluids, the volume concentration of nanoparticles and their thermal conductivity coefficient have the main effect [35,53,77,84,89,95,114,132,150,158].

The fluid is coming into motion under the influence of volumetric and surface forces. Volumetric forces occur as a result of the fluid density gradient. The surface forces are caused by a local change in the surface tension of the fluid, which is mainly associated with the appearance of a nonuniform distribution of the bulk temperature or concentration of nanoparticles on the surface, which is, as a rule, a consequence of a change in their thermodynamic state in the fluid volume (the Marangoni effect).

Concentration-capillary convection contains several new hydrodynamic effects caused by the concentration inhomogeneity of nano-heat carriers close to the surfaces of the cooling channel. This facilitates the appearance of bubbles and drops near the microroughness of their surfaces. The structure of nanocarriers movement in the cavity of the cooling channel depends on its shape, configuration, and mechanical cleanliness of the cavity surface, as well as on the location in the area of the heated engine cylinder head.

In this case, surface forces prevail over volume forces arising in nano-heat carriers. This condition is typical for thin horizontal layers and films of fluid, near the surface of droplets and air bubbles in the fluid. There are two main factors to consider. The first factor is that the specific time of heat diffusion is hundreds and even thousands of times shorter than the time of existence of concentration inhomogeneities. As a result, the latter exist much longer in fluids than the thermal ones, and their duration and action intensity of capillary forces at the interface increases many times. This promotes the intensification of heat removal from the nano-heat carriers to the walls of the channel cavity. The second factor is the adsorption of nanoparticles on the fluid surface, which promotes the concentration-capillary drift of air bubbles. The action of Marangoni forces on the free fluid surface causes its movement in the direction of increasing surface tension. The surface lugs away the adjacent layers of liquid. As a result, if the free surface belongs to the bubble, it begins to be displaced in the direction opposite to the liquid flow. This ability of air bubbles to spontaneously move in the fluid in the direction of decreasing surface tension causes their capillary drift [73,78,85,95,109,128,136,151].

7. Devices with Nanoparticles in the Engine Cylinder Head Cooling System

If bubbles are located on a horizontal liquid layer bounded at the top and sides of the channel walls, such conditions suppress their floatation.

The action of the condensation-capillary effect is observed only for a limited time, determined by the rate of the adsorption process.

Let us note that in the thermal version of the problem of fluid motion near stationary bubbles and drops, only its stationary flow develops (the ratio of the kinematic viscosity and thermal diffusivity coefficients, as a rule, does not exceed one order of magnitude).

It has been established that as soon as the ascending capillary movement of the bubble over the surface stops, the dynamic equilibrium of the concentration “cap” (as being heavier than the surrounding liquid) is violated. The restoration of the difference in the concentration of nano-heat carriers between the poles of the bubble again activates capillary forces, which contribute to a sharp acceleration of the upward current. As a result, an intense convective liquid motion occurs at the side surface of the cylindrical bubble due to the appearance of two symmetric vortices. While developing, vortex cells capture an increasing volume of liquid with a high concentration of nanoparticles. Due to this, the average density of the nano-heat carrier in the cells increases, and they move downward, cutting off the liquid stream from the lower pole of the cells, which backs up its movement [74,92,113,129,135,149,156].

Displacement of electrons in powder particles under the action of a temperature field goes with potential energy of interaction between polarized charges particles:

$$U_e = -qN(\varphi^+ - \varphi^-)/2 \quad (2)$$

here, q —the average charge rate of the dipoles; N —algebraic sum in 1 m^3 ; φ^+ and φ^- —self-consistent of positive and negative the average value of the charges of the dipoles; accepting the Gibbs-Helmholtz equation is a thermodynamic equation $U = F - T\left(\frac{\partial F}{\partial T}\right)_V$ and equality in partial derivatives; partial differential $\left(\frac{\partial F}{\partial T}\right)_V = 0$, we come up with $U_e = F$, position F —free energy of polarized nanoparticles. T —temperature.

Due to the local nature electric fields of nanoparticles polarized and the long-range action of the Coulomb synergistic, a drastic change in the polarization charge of one of the particles goes with a change in the potential energy (Figure 4) of the powder U_e and hence a significant change in the state of all electrons in the system. Accordingly, it is probable to have conditions under which all free electrons of the powder nanoparticles participate in the exchange correlation function synergistic and provide a single system.

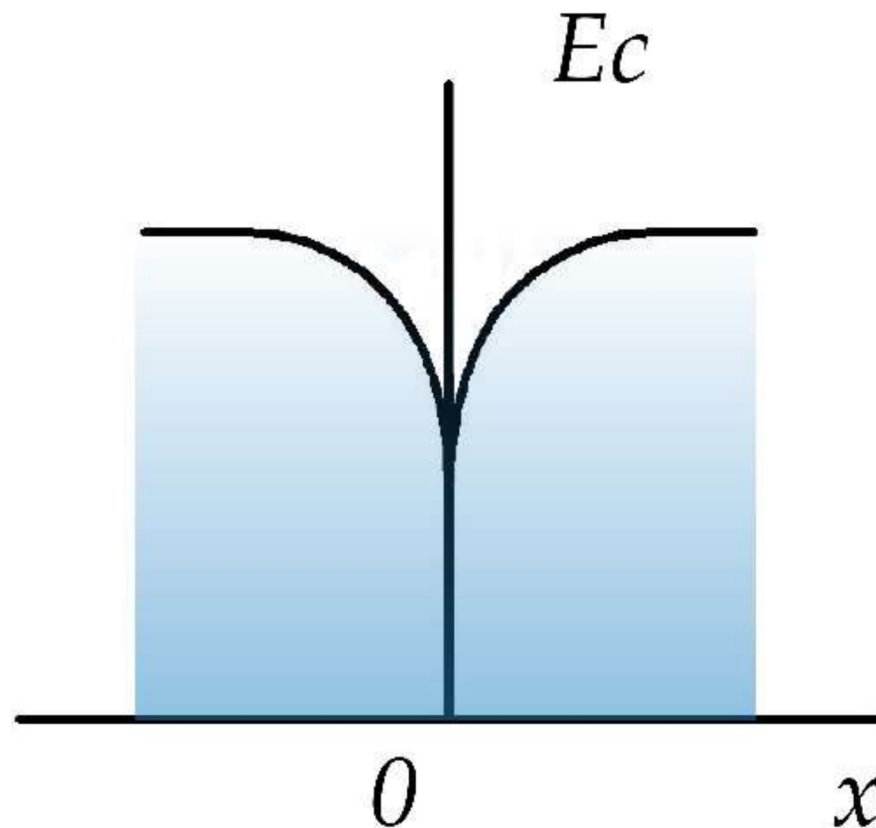


Figure 4. Dependence of conduction electrons potential energy in the powder particles on the x coordinate directed along the plane of their contact, $x = 0$.

Forced radiation of a thermodynamic system to a permanent state corresponds to a reduction of its inside (adiabatic process) or free energy (isothermal process) of a thermodynamic system.

Nanoparticles' spontaneous polarization with area donor centers situated on the surface of its nanoparticles can be circumspect as a transition phase in the powder electron subsystem to a state whereabouts $F < 0$.

The role of contacts between powder nanoparticles in the exchange–correlation function synergistic of their free electrons is obvious by the incoming experimental results.

If globular nickel or aluminum oxide nanoparticles are located between the powder microparticles using an accurately mixed mixture of micro- and nanoparticles, then under the same conditions, the state of spontaneous polarization of the $KMnO_4$ powder with chemisorbed hydrogen does not appear.

In this case, due to the lack of direct contacts between microparticles, free electrons belong to different particles, the exchange–correlation interaction between them is loosened, so the status $F < 0$ is not contented.

Therefore, the donor centers its position on the surface of powder nanoparticles given the emergence of self-consistent states of free electrons connected with their common potential wells in the area of contacts between microparticles.

Powder nanoparticles comprise positively loaded donor centers on their area, generating area bending of the zones.

It was fixed that the insertion of light and heavy nanoparticles of aluminum oxide Al_2O_3 into the water in a mass concentration of 0.75% led to a magnification in its thermal conductivity coefficient by 60% compared to the base fluid at a coolant temperature of 90 °C, which matches the operating temperature of the engine cooling systems.

At the shown temperature, the base fluid has a thermal conductivity coefficient of $0.545 \frac{W}{(m \times ^\circ C)}$; for nanofluid with Al_2O_3 nanoparticles its meaning was $0.872 \frac{W}{(m \times ^\circ C)}$.

Let us view a powder model in the form of a nanoparticles chain. We will suppose that the outermost nanoparticles of the chain are in contact with a spherical dielectric.

When a powder is polarized by a temperature field, free electrons of the nanoparticles are crowded out under the action of the field.

Opposite polarization charges located on opposite boundaries of the particles chain create an additional field inside the powder, the intensity vector E_p of which is directed in the same way as the intensity vector of the temperature field of the liquid E_0 (Figure 5b).

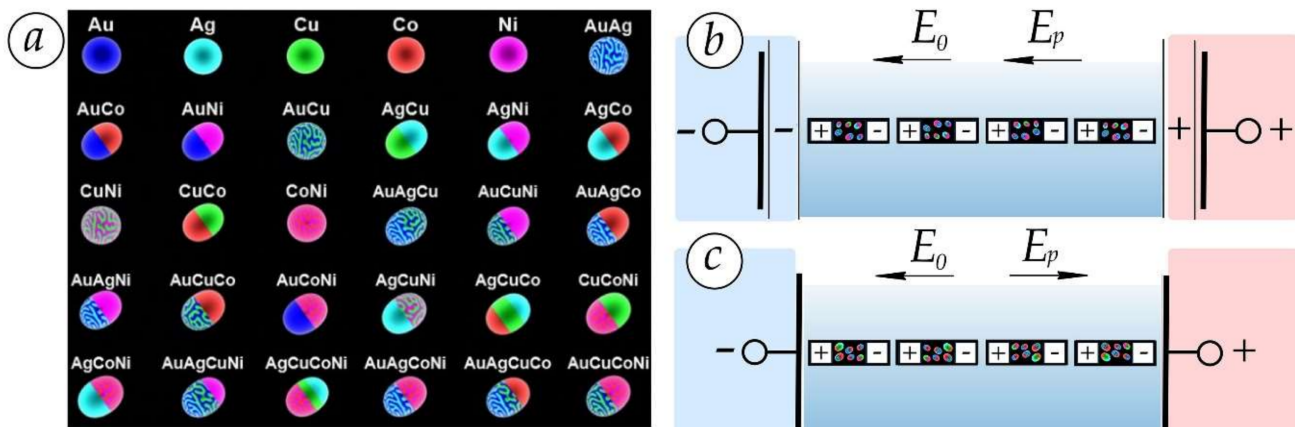


Figure 5. Unary, binary, ternary, and quaternary types of nanoparticles synthesized for industrial application [166] (a). Model of a powder in the form of grouped particles chain, the outermost of which are in interaction with devices that have nanoparticles coated with dielectric (b) and metal (c) shells.

Consequently, the following conditions are met:

$$E = E_0 + E_p = E_0 + \aleph E = \frac{E_0}{(1 - \aleph)} \quad (3)$$

where, E —field density in nanoparticle; E_0 —temperature field density; E_p —field density of polarizing charges located at counter boundaries of the nanoparticle grade; \aleph —its dielectric impressionability. Let us denote $1 - \aleph = e$. We can assume that the ε value is a macroscopic characteristic of the powder if referable to the connection among its particles, the free electrons of the powder form a single system. The amount ε will be called the static dielectric constant of the powder. Consequently to the Kramers–Kronig dispersion bonds, one of the provision $\varepsilon \geq 1$; $\varepsilon \leq 0$ is complacent for the static dielectric constant of a random field-polarized material. Accordingly, using the expression $1 - \aleph = e$, where $\aleph > 0$ for the static dielectric constant of the powder, we obtain $\varepsilon < 0$.

According to Figure 5c, the energy level of the nanofluid will be weakened since its components are directed in different directions.

Figure 6a–c shows device schemes stuffed with nanoparticles with different densities, which act as local heat exchangers at different levels of nanofluid driving flow. The dimensions of the devices depend on the reduced diameter of the cooling channel. Nanoparticle devices can have a polymer coating on one of the shells.

According to Figure 6b, if the fluid absorption occurs from below and by dry nanoparticles of a spherical device, then the radius of the widest hole should be taken; if absorption occurs from above or the body has been pre-wetted, then the radius of the narrowest part of the hole should be taken.

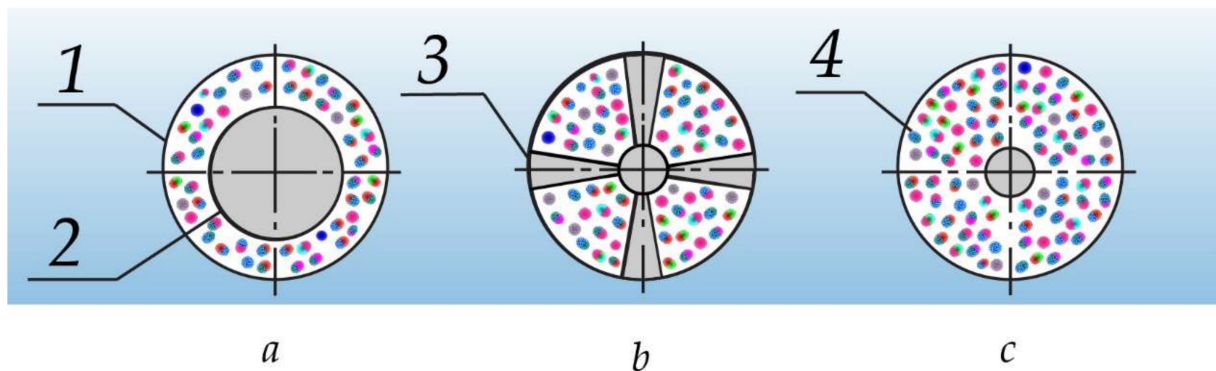


Figure 6. Structure diagrams of devices made of various weights nanoparticles, in the form of (a)—washers with an inner hole; (b,c)—spherical shape with diffusers and nanoparticles; 1 and 2—outer and inner shell; 3—diffuser holes; 4—nanoparticles.

Adding to water of aluminum oxide Al_2O_3 “light” and “heavy” nanoparticles in a mass concentration of 0.75% led to an increase of its thermal conductivity coefficient by 60% compared to the base fluid at a coolant temperature of 90 °C, which is characteristic of the engine cooling systems operating temperature. Thus, at the indicated temperature, the base fluid had thermal conductivity coefficient of $0.545 \frac{W}{(m \times ^\circ C)}$, while for nanofluid with Al_2O_3 its value was $0.872 \frac{W}{(m \times ^\circ C)}$, i.e., increased by 58.0%. At the same time, a parameter change of the nanofluid in engine cooling system was achieved; average travel speed from 0.2 dL to 2.0 $\frac{m}{s}$; average temperature 65–90 °C; heat flux density 2×10^2 – $2 \times 10^6 \frac{W}{m^2}$; heat transfer coefficient 150–1000 $\frac{W}{(m^2 \times ^\circ C)}$; heat transfer coefficient 100–750 $\frac{W}{(m^2 \times ^\circ C)}$.

Therefore, it has been established that nanoparticles of the same or different chemical composition, introduced into devices of various shapes and masses, physically interact with each other. The choice of a device that is a local heat exchanger depends on the shape of the cooling system chamber and the thermodynamic state of the base fluid. Devices with nanoparticles can be given additional effects: diffuser, confuser, thermoelectric, etc. Local heat exchangers without a base fluid enhance the Peltier effect by reducing the amount of Joule heat in the branch of the thermoelectric cooler. Nanofluids can be used in heat exchange systems for cooling machines and units for various purposes: in disc-shoe brakes of hoisting machines, in self-ventilated disc-shoe brakes of vehicles, in tape-shoe brake pulleys of drawworks. In this case, hydrogen containing cooling systems with nanoparticles can be stationary and rotating. So far, nanoparticles have been used in engine oil, transmission oil, and radiator coolant to enhance heat transfer removal from vehicle engines [182].

8. Conclusions

The results of theoretical and experimental studies of nanofluids and devices made of nanoparticles of various weights in the cylinder head cooling system allow us to state the following:

- an increase of the cooling nanofluid thermal conductivity coefficient is determined by a change in the mass concentration of aluminum oxide nanoparticles in the base fluid. This will make it possible to create coolants with such thermophysical characteristics that are required to ensure intensive heat exchange in engine cooling systems of various capacities;
- a viscosity has been achieved, at which, on the one hand, losses of nanofluid through all kinds of seals and connecting nodes will be excluded, and, on the other hand, significant power consumption will not be required for pumping the nano-heat carrier through the engine cooling system;
- the set of gradients in the carrier stream of nanofluids should provide them with such a boiling point that will be 25–30 °C higher than the maximum allowable temperature

- of the nano-heat carrier in the cooling system, which will prevent the appearance of air-vapor cork in it and reduce losses of the nano-heat carrier during evaporation due to local heat exchangers, i.e., devices with nanoparticles;
- the possibility to provide a needed engine temperature mode with a relatively small volume of nano-heat carrier circulating in the cooling system is ensured by a high specific heat capacity;
 - thermodynamics and molecular kinetic theory complement each other, the same theoretical and experimental material is a subject to synthesis and complex analysis; moisture transfer is inseparable from heat transfer and the phenomenon of heat and mass transfer must be considered in its inseparable connection: therefore, it is proposed to introduce a new concept “potential of heat-conducting transfer by nanoparticles in a fluid”.
 - it has been established the role of contacts between powder parts in the exchange–correlation interaction of their free electrons is evidenced by the following experimental results. If spherical nickel or aluminum oxide nanoparticles are placed between the powder microparticles using a thoroughly mixed mixture of micro- and nanoparticles, then under the same conditions, the state of spontaneous polarization of the $KMnO_4$ powder with chemisorbed hydrogen does not appear.
 - Thus, the permissible temperature level of internal combustion engines is ensured by intensifying heat transfer in cooling systems due to the modification of coolants with “light” and “heavy” nanoparticles.

Author Contributions: The scope of work of individual authors during the performance of this project was the same. The authors performed the study together and then analyzed its findings. The paper was written together. The authors equally contributed to the paper assembly. Partially: conceptualization, A.B., V.K. and K.F.A.; data curation, O.B., D.V. and V.S.; formal analysis, D.Z., I.B., V.K. and M.O.; investigation, A.B., M.K. and K.F.A.; methodology, A.B., O.B., K.F.A. and M.K.; writing—original draft, A.B.; writing—review and editing, A.B. and K.F.A. All authors have read and agreed to the published version of the manuscript.

Funding: This research was partially funded by the NCBR (Poland) and A.B. acknowledges for their partial support in the framework of project POIR.04.01.04-00-0040/20 “Development of an intelligent and maintenance-free system for stabilizing the operation of electricity distribution networks based on modular installations of a hydrogen energy buffer with the intention of utilizing hydrogen”.

Institutional Review Board Statement: Not applicable.

Informed Consent Statement: Informed consent was obtained from all subjects involved in the study.

Data Availability Statement: Not applicable.

Conflicts of Interest: The authors declare no conflict of interest, we do not have any personal conflicts of interest in communicating the findings of this study, and we had no sponsor who would make claims to the findings being presented.

Nomenclature and Abbreviations

λ	thermal conductivity coefficient,
λ_0	thermal conductivity coefficient of base fluid,
Q	the amount of heat,
T	temperature,
P	pressure,
V	specific volume,
q	specific heat flux,
T_s	bulk liquid saturation temperature,
T_f	saturation temperature,
T_w	wall temperature,
ΔT_{sub}	$\Delta T_{sub} = T_s - T_f$.—underheating,

BNB	the beginning of nucleate boiling,
DNB	the development of nucleate boiling,
CHF	point of critical heat flow,
TEC	thermo electric cooler,
x	mass steam quality,
x_b	the relative enthalpy of the flow,
h_f	specific enthalpy of the flow,
h'	specific enthalpy of liquid in saturation state,
r	specific heat of vaporization,
q_{cg2}	position of the second boiling crisis,
ΔT_{cg2}	position of the second boiling crisis,
φ	the volume concentration,
λ_{nf}	thermal conductivity coefficients of the nanofluid,
λ_{bf}	conductivity coefficients of the base fluid,
φ_m	mass concentration of nanoparticles in the base liquid,
s	specific surface area,
U_e	displacement of electrons in powder particles,
q	average value of dipoles charges,
N	number of particles in 1 m^3 ,
φ^+ and φ^-	self-consistent potentials of positively and negatively charged regions of particles created by all charges of the system,
E	field density in powder,
E_0	temperature field density,
E_p	field density of polarizing charges located at opposite boundaries of the powder layer,
\aleph	dielectric susceptibility,
λ	thermal conductivity coefficient of suspensions.

References

- Sharoglazov, B.A.; Farafontov, M.F.; Klement'ev, V.V. *Internal Combustion Engines: Theory, Modeling and Calculation of Processes*; South Ural University Publisher: Chelyabinsk, Russia, 2005; 403p.
- Balitski, A.; Krohmalny, O.; Ripey, I. Hydrogen cooling of turbogenerators and the problem of rotor retaining ring materials degradation. *Int. J. Hydrogen Energy* **2000**, *25*, 167–171. [\[CrossRef\]](#)
- Kavtaradze, R.Z. *Local Heat Exchange in Piston Engines*; MGTU im. N.E. Bauman: Moscow, Russia, 2007; 472p.
- Shabanov, A.Y.; Zaitsev, A.B.; Mashkur, M.A. A new method for calculating the boundary conditions for thermal loading of the cylinder head of a piston engine. *Dvigatelsestroyeniye* **2005**, *1*, 5–9.
- Chainov, N.D.; Obolonnyi, I.V.; Sidorov, A.A. To the issue of physical modeling of the thermal state of parts of the engine cylinder-piston group. *Izv. VUZov Mech. Eng.* **1989**, *2*, 69–72.
- Pekhovich, A.I.; Liquid, V.M. *Calculations of the Thermal Mode of Solids*; Energiya: Leningrad, Russia, 1976; 352p.
- Muchnik, G.F.; Rubashov, I.B. *Methods of the Heat Transfer Theory: Thermal Radiation*; Higher School: Moscow, Russia, 1974; 272p.
- Tsvetkov, F.F.; Grigoriev, B.A. *Heat and Mass Transfer*; Publishing House of MEI: Moscow, Russia, 2005; 215p.
- Shekhovtsov, A.F. *Mathematical Modeling of Heat Transfer in High-Speed Diesel Engines*; Vishcha shkola: Kharkov, Russia, 1978; 153p.
- Heywood, J.B. *Internal Combustion Engine Fundamentals*; McGraw-Hill: New York, NY, USA, 1988; 960p.
- Kawiak, M.; Balitskii, A. Embrittlement of welded joints of tram rails in city environments. *Eng. Fail. Anal.* **2018**, *85*, 97–103. [\[CrossRef\]](#)
- Dzhanakhmedov, A.K.; Skrypnyk, V.S.; Dolishniy, B.V.; Volchenko, N.A.; Nikipchuk, S.B.; Wudwud, A.N. Thermal balance of internal combustion engines and methods of reducing heat losses. *Bull. Azerbaijan Eng. Acad.* **2021**, *13*, 32–41.
- Rudyak, V.Y.; Minakov, A.V.; Pryazhnikov, M.I. Thermophysical properties of nanofluids and similarity criteria. *Lett. J. Tech. Phys.* **2016**, *42*, 9–16.
- Gorshkov, R.V. Ensuring the Permissible Temperature Level of Forced Ship Diesel Engines by Intensifying Heat Transfer in Cooling Systems due to the Modification of Coolants with Nanoparticles. Ph.D. Thesis, Yaroslavl University, Yaroslavl, Russia, 2019; p. 127.
- Rudyak, V.Y. *Statistical Aerohydromechanics of Homogeneous and Heterogeneous Media: T. 2. Hydromechanics*; NGASU: Novosibirsk, Russia, 2005; 468p.
- Ding, Y.; Chen, H.; Wang, L.; Yang, C.Y.; He, Y.; Yang, W.; Lee, W.P.; Zhang, L.; Huo, H. Heat transfer intensification using nanofluids. *KONA Powder Part. J.* **2007**, *25*, 23–38. [\[CrossRef\]](#)
- Wang, X.; Xu, X.; Choi, S.U.S. Thermal conductivity of nanoparticlefluid mixture. *J. Thermophys. Heat Trans.* **1999**, *13*, 474–480. [\[CrossRef\]](#)
- Maxwell, J.C.A. *Treatise on Electricity and Magnetism*, 2nd ed.; Clarendon Press: Oxford, UK, 1881; Volume 1, 435p.

19. Eastman, J.A.; Choi, S.U.S.; Li, S.; Thompson, L.J.; Lee, S. Enhanced thermal conductivity through the development of nanofluids. In *Materials Research Society; Fall Meeting*: Boston, MA, USA, 1998; pp. 3–11.
20. Ropyak, L.Y.; Shatskiy, I.P.; Prytula, I.M.; Gryn, L.O.; Belyakovskiy, V.O. Stressed state of laminated interference-absorption filter under local loading. *Funct. Mater.* **2020**, *27*, 638–642.
21. Malanchuk, N.; Martynyak, R.; Monastyrskyy, B. Thermally induced local slip of contacting solids in vicinity of surface groove. *Int. J. Solids Struct.* **2011**, *48*, 1791–1797. [[CrossRef](#)]
22. Balitskii, O.A.; Savchyn, V.P.; Savchyn, P.V. Thermal oxidation of indium and gallium sulphides. *Phys. B Condens. Matter* **2005**, *355*, 365–369. [[CrossRef](#)]
23. Balitskii, O.; Borowiak-Palen, E.; Konicki, W. Synthesis and characterization of colloidal gallium selenide nanowires. *Cryst. Res. Technol.* **2011**, *46*, 417–420. [[CrossRef](#)]
24. Balitskii, A.; Mochulskiy, V.; Ivaskovich, L.; Elias, J.; Skolozdra, O. Influence of high pressure and high temperature hydrogen on fracture toughness of Ni-containing steels and alloys. *Arch. Mech. Eng.* **2014**, *LXI*, 129–138. [[CrossRef](#)]
25. Balitskii, O.A. Recent energy targeted applications of localized surface plasmon resonance semiconductor nanocrystals: A mini-review. *Mater. Today Energy* **2021**, *20*, 100629. [[CrossRef](#)]
26. Balitskii, O.A.; Kolesnikov, V.O.; Balitskii, A.I. Wear resistance of hydrogenated high nitrogen steel at dry and solid state lubricants assistant friction. *Arch. Mater. Sci. Eng.* **2019**, *2*, 57–67. [[CrossRef](#)]
27. Balitskii, A.A.; Kolesnikov, V.A.; Vus, O.B. Tribotechnical properties of nitrogen manganese steels under rolling friction at addition of (GaSe)_xIn_{1-x} powders into contact zone. *Metallofiz. I Noveishie Tekhnologii* **2010**, *32*, 685–695.
28. Osenin, Y.I.; Sosnov, I.I.; Chesnokov, A.V.; Antoshkina, L.I.; Osenin, Y.Y. Friction Unit of a Disc Brake Based on a Combination of Friction Materials. *J. Frict. Wear* **2019**, *40*, 293–296. [[CrossRef](#)]
29. Osenin, Y.I.; Krivosheya, Y.V.; Chesnokov, A.V.; Antoshkin, V.K. Influence of the Mutual Overlapping Coefficient on the Process of a Disc Brake Squealing during Braking. *J. Frict. Wear* **2021**, *42*, 38–43. [[CrossRef](#)]
30. Sander, D.E.; Allmaier, H.; Priebsch, H.H.; Witt, M.; Skiadas, A. Simulation of journal bearing friction in severe mixed lubrication—Validation and effect of surface smoothing due to running-in. *Tribol. Int.* **2016**, *96*, 173–183. [[CrossRef](#)]
31. Balyts'kyi, O.I.; Kolesnikov, V.O. Investigation of wear products of high-nitrogen manganese steels. *Mater. Sci.* **2009**, *45*, 576–581. [[CrossRef](#)]
32. Balyts'kyi, O.I.; Abramek, K.F.; Mruzik, M.; Shtoeck, T.; Osipowicz, T. Evaluation of the losses of hydrogen-containing gases in the process of wear of pistons of an internal-combustion engine. *Mater. Sci.* **2017**, *53*, 289–294. [[CrossRef](#)]
33. Hu, S.; d'Ambrosio, S.; Finesso, R.; Manelli, A.; Marzano, M.R.; Mittica, A.; Ventura, L.; Wang, H.; Wang, Y. Comparison of physics-based, semi-empirical and neural network-based models for model-based combustion control in a 3.0 L diesel engine. *Energies* **2019**, *12*, 3423. [[CrossRef](#)]
34. Dorscheidt, F.; Pischinger, S.; Claßen, J.; Sterlepper, S.; Krysmo, S.; Görgen, M.; Nijs, M.; Straszak, P.; Abdelkader, A.M. Development of a novel gasoline particulate filter loading method using a burner bench. *Energies* **2021**, *14*, 4914. [[CrossRef](#)]
35. Żółtowski, A.; Gis, W. Ammonia emissions in SI engines fueled with LPG. *Energies* **2021**, *14*, 691. [[CrossRef](#)]
36. Cubito, C.; Millo, F.; Boccardo, G.; Di Pierro, G.; Ciuffo, B.; Fontaras, G.; Serra, S.; Otura Garcia, M.; Trentadue, G. Impact of different driving cycles and operating conditions on CO₂ emissions and energy management strategies of a Euro-6 hybrid electric vehicle. *Energies* **2017**, *10*, 1590. [[CrossRef](#)]
37. Feru, E.; Willems, F.; De Jager, B.; Steinbuch, M. Modeling and control of a parallel waste heat recovery system for euro-VI heavy-duty diesel engines. *Energies* **2014**, *7*, 6571–6592. [[CrossRef](#)]
38. Attaphong, C.; Sabatini, D.A. Phase Behaviors of vegetable oil-based microemulsion fuels: The effects of temperatures, surfactants, oils, and water in ethanol. *Energy Fuels* **2013**, *27*, 6773–6780. [[CrossRef](#)]
39. Dmytrakh, I.M.; Leshchak, R.L.; Syrotyuk, A.M.; Barna, R.A. Effect of hydrogen concentration on fatigue crack growth behaviour in pipeline steel. *Int. J. Hydrogen Energy* **2017**, *42*, 6401–6408. [[CrossRef](#)]
40. Belov, S.V. *Environmental Protection*; Higher School Publisher House: Moscow, Russia, 1991; 319p.
41. Karpuschewski, B.; Welzel, F.; Risse, K.; Matthias Schorgel, M.; Kreter, S. Potentials for improving efficiency of combustion engines due to cylinder liner surface engineering. *Procedia CIRP* **2016**, *46*, 258–265. [[CrossRef](#)]
42. Borowski, T.; Kulikowski, K.; Adamczyk-Cieślak, B.; Roźniatowski, K.; Szychalski, M.; Tarnowski, M. Influence of nitrided and nitrocarburised layers on the functional properties of nitrogen-doped soft carbon-based coatings deposited on 316L steel under DC glow-discharge conditions. *Surf. Coat. Technol.* **2020**, *392*, 125705. [[CrossRef](#)]
43. Balyts'kyi, O.I.; Kolesnikov, V.O.; Elias, Y.; Havrylyuk, M.R. Specific features of the fracture of hydrogenated high-nitrogen manganese steels under conditions of rolling friction. *Mater. Sci.* **2015**, *50*, 604–611. [[CrossRef](#)]
44. Balyts'kyi, O.I.; Kolesnikov, V.O.; Havrylyuk, M.R. Influence of lubricating liquid on the formation of the products of cutting of 38KhN3MFA steel. *Mater. Sci.* **2019**, *54*, 722–727. [[CrossRef](#)]
45. Balyts'kyi, O.I.; Kolesnikov, V.O.; Elias, J. Study of the wear resistance of high-nitrogen steels under dry sliding friction. *Mater. Sci.* **2013**, *48*, 642–646. [[CrossRef](#)]
46. Balyts'kyi, O.I.; Kolesnikov, V.O.; Kubicki, E. Enhancement of the crack resistance of manganese cast irons. *Mater. Sci.* **2005**, *41*, 67–73. [[CrossRef](#)]
47. Balyts'kyi, O.I.; Kolesnikov, V.O. Investigation of the wear products of austenitic manganese cast irons. *Mater. Sci.* **2004**, *40*, 78–82. [[CrossRef](#)]

48. Balyts'kyi, O.I.; Chniel, J.; Dorobczynski, L. Analysis of electrochemical oscillations under conditions of vibration cavitation. *Mater. Sci.* **2011**, *47*, 21–25. [[CrossRef](#)]
49. Balitskii, O.A.; Kolesnikov, V.O.; Balitskii, A.I.; Eliaszyk, J.J.; Havrylyuk, M.R. Hydrogen effect on the high-nickel surface steel properties during machining and wear with lubricants. *Arch. Mater. Sci. Eng.* **2020**, *104*, 49–57. [[CrossRef](#)]
50. Kindrachuk, M.; Volchenko, D.; Balitskii, A.; Abramek, K.F.; Volchenko, M.; Balitskii, O.; Skrypnyk, V.; Zhuravlev, D.; Yurchuk, A.; Kolesnikov, V. Wear Resistance of spark ignition engine piston rings in hydrogen-containing environments. *Energies* **2021**, *14*, 4801. [[CrossRef](#)]
51. Balitskii, O.; Kolesnikov, V. Identification of wear products in the automotive tribotechnical system using computer vision methods, artificial intelligence and big data. In Proceedings of the XIth International Scientific and Practical Conference on Electronics and Information Technologies (ELIT), Ukraine, Russia, 16–18 September 2019; pp. 24–27.
52. Jamrozik, A.; Tutak, W.; Grab-Rogalski, K. Combusting stability, performance and emission characteristics of a CI engine fueled with diesel/n-butanol blends. *Energies* **2021**, *14*, 2817. [[CrossRef](#)]
53. Kindrachuk, M.V.; Vol'chenko, D.A.; Vol'chenko, N.A.; Stebeletskaya, N.M.; Voznyi, A.V. Influence of hydrogen on the wear resistance of materials in the friction couples of braking units. *Mater. Sci.* **2017**, *53*, 282–288. [[CrossRef](#)]
54. Hussain, A.; Arshad, M.; Rehman, A.; Hassan, A.; Elagan, S.K.; Ahmad, H.; Ishan, A. Three-dimensional water-based magneto-hydrodynamic rotating nanofluid flow over a linear extending sheet and heat transport analysis: A numerical approach. *Energies* **2021**, *14*, 5133. [[CrossRef](#)]
55. Hayat, T.; Nadeem, S. An improvement in heat transfer for rotating flow of hybrid nanofluid: A numerical study. *Can. J. Phys.* **2018**, *96*, 1420–1430. [[CrossRef](#)]
56. Hayat, T.; Nadeem, S.; Khan, A.U. Rotating flow of Ag-CuO/H₂O hybrid nanofluid with radiation and partial slip boundary effects. *Eur. Phys. J. E* **2018**, *41*, 75. [[CrossRef](#)] [[PubMed](#)]
57. Nadeem, S.; Rehman, A.; Mehmood, R.; Sadiq, M. Partial Slip effects on a rotating flow of two phase nano fluid over a stretching surface. *Curr. Nanosci.* **2014**, *10*, 846–854. [[CrossRef](#)]
58. Aslani, K.-E.; Mahabaleshwar, U.S.; Singh, J.; Sarris, I.E. Combined effect of radiation and inclined MHD flow of a micropolar fluid over a porous stretching/shrinking sheet with mass transpiration. *Int. J. Appl. Comput. Math.* **2021**, *7*, 60. [[CrossRef](#)]
59. Bahiraei, M.; Hosseinalipour, S.M.; Hangi, M. Numerical study and optimization of hydrothermal characteristics of Mn-Zn ferrite nanofluid within annulus in the presence of magnetic field. *J. Superconduct. Novel Magn.* **2014**, *27*, 527–534. [[CrossRef](#)]
60. Shahid, A.; Huang, H.L.; Khalique, C.M.; Bhatti, M.M. Numerical analysis of activation energy on MHD nanofluid flow with exponential temperature-dependent viscosity past a porous plate. *J. Therm. Anal. Calorim.* **2021**, *143*, 2585–2596. [[CrossRef](#)]
61. Ahmad, S.; Nadeem, S.; Ullah, N. Entropy generation and temperature-dependent viscosity in the study of SWCNT-MWCNT hybrid nanofluid. *Appl. Nanosci.* **2020**, *10*, 5107–5511. [[CrossRef](#)]
62. Rizwana, R.; Hussain, A.; Nadeem, S. Mix convection non-boundary layer flow of unsteady MHD oblique stagnation point flow of nanofluid. *Int. Commun. Heat Mass Transf.* **2021**, *124*, 105285. [[CrossRef](#)]
63. Moustabchir, H.; Azari, Z.; Hairi, S.; Dmytrakh, I. Experimental and computed stress distribution ahead of notch in pressure vessel: Application of T-stress conception. *Comput. Mater. Sci.* **2012**, *58*, 59–66. [[CrossRef](#)]
64. Shafiq, A.; Rasool, G.; Khalique, C.M. Significance of thermal slip and convective boundary conditions in three dimensional rotating darcy-forchheimer nanofluid flow. *Symmetry* **2020**, *12*, 741. [[CrossRef](#)]
65. Waini, I.; Ishak, A.; Pop, I. Unsteady flow and heat transfer past a stretching/shrinking sheet in a hybrid nanofluid. *Int. J. Heat Mass Transf.* **2019**, *136*, 288–297. [[CrossRef](#)]
66. Hussain, A.; Alshbool, M.H.; Abdussattar, A.; Rehman, A.; Ahmad, H.; Nofal, T.A.; Khan, M.R. A computational model for hybrid nanofluid flow on a rotating surface in the existence of convective condition. *Case Stud. Therm. Eng.* **2021**, *27*, 101089. [[CrossRef](#)]
67. Hussain, A.; Hassan, A.; Al Mdallal, Q.; Ahmad, H.; Rehman, A.; Altanji, M.; Arshad, M. Heat transport investigation of magneto-hydrodynamics (SWCNT-MWCNT) hybrid nanofluid under the thermal radiation regime. *Case Stud. Therm. Eng.* **2021**, *27*, 101244. [[CrossRef](#)]
68. Nasirzadehroshenin, F.; Sadeghzadeh, M.; Khadang, A.; Maddah, H.; Ahmadi, M.H.; Sakhaeina, H.; Chen, L. Modeling of heat transfer performance of carbon nanotube nanofluid in a tube with fixed wall temperature by using ANN-GA. *Eur. Phys. J. Plus* **2020**, *135*, 217. [[CrossRef](#)]
69. Sheikholeslami, M.; Bhatti, M. Active method for nanofluid heat transfer enhancement by means of EHD. *Int. J. Heat Mass Transf.* **2017**, *109*, 115–122. [[CrossRef](#)]
70. Cheng, L. Nanofluid heat transfer technologies. *Recent Pat. Eng.* **2009**, *3*, 1–7. [[CrossRef](#)]
71. Afrand, M. Using a magnetic field to reduce natural convection in a vertical cylindrical annulus. *Int. J. Therm. Sci.* **2017**, *118*, 12–23. [[CrossRef](#)]
72. Choi, S.U.; Eastman, J.A. *Enhancing Thermal Conductivity of Fluids with Nanoparticles*; No. ANL/MSD/CP-84938, CONF-951135-29; Argonne National Laboratory: Lemont, IL, USA, 1995; 250p.
73. Hussain, A.; Arshad, M.; Rehman, A.; Hassan, A.; Elagan, S.K.; Alshehri, N.A. Heat transmission of engine-oil-based rotating nanofluids flow with influence of partial slip condition: A Computational model. *Energies* **2021**, *14*, 3859. [[CrossRef](#)]
74. Abbas, W.; Magdy, M.M. Heat and mass transfer analysis of nanofluid flow based on, and over a moving rotating plate and impact of various nanoparticle shapes. *Math. Prob. Eng.* **2020**, *2020*, 9606382. [[CrossRef](#)]

75. Khan, N.S.; Shah, Q.; Bhaumik, A.; Kumam, P.; Thounthong, P.; Amiri, I. Entropy generation in bioconvection nanofluid flow between two stretchable rotating disks. *Sci. Rep.* **2020**, *10*, 4448. [\[CrossRef\]](#)
76. Elcioglu, E.B. A High-Accuracy Thermal conductivity model for water-based graphene nanoplatelet nanofluids. *Energies* **2021**, *14*, 5178. [\[CrossRef\]](#)
77. Zhou, Y.; Cui, X.; Weng, J.; Shi, S.; Han, H.; Chen, C. Experimental investigation of the heat transfer performance of oscillating heat pipe with graphene nanofluids. *Powder Technol.* **2018**, *332*, 371–380. [\[CrossRef\]](#)
78. Arzani, H.K.; Amiri, A.; Kazi, S.N.; Chew, B.T.; Badarudin, A. Experimental and numerical investigation of thermophysical properties, heat transfer and pressure drop of covalent and noncovalent functionalized graphene nanoplatelet-based water nanofluids in an annular heat exchanger. *Int. Commun. Heat Mass Transf.* **2015**, *68*, 267–275. [\[CrossRef\]](#)
79. Keklikcioglu, O.; Dagdevir, T.; Ozceyhan, V. Heat transfer and pressure drop investigation of graphene nanoplatelet-water and titanium dioxide-water nanofluids in a horizontal tube. *Appl. Therm. Eng.* **2019**, *162*, 114256. [\[CrossRef\]](#)
80. Iranmanesh, S.; Ong, H.C.; Ang, B.C.; Sadeghinezhad, E.; Esmaeilzadeh, A.; Mehrali, M. Thermal performance enhancement of an evacuated tube solar collector using graphene nanoplatelets nanofluid. *J. Clean. Prod.* **2017**, *162*, 121–129. [\[CrossRef\]](#)
81. Sadeghinezhad, E.; Mehrali, M.; Rosen, M.A.; Akhiani, A.R.; Latibari, S.T.; Mehrali, M.; Metselaar, H.S.C. Experimental investigation of the effect of graphene nanofluids on heat pipe thermal performance. *Appl. Therm. Eng.* **2016**, *100*, 775–787. [\[CrossRef\]](#)
82. Mehrali, M.; Sadeghinezhad, E.; Rosen, M.A.; Latibari, S.T.; Mehrali, M.; Metselaar, H.S.C.; Kazi, S.N. Effect of specific surface area on convective heat transfer of graphene nanoplatelet aqueous nanofluids. *Exp. Therm. Fluid Sci.* **2015**, *68*, 100–108. [\[CrossRef\]](#)
83. Ali, H.M.; Arshad, W. Effect of channel angle of pin-fin heat sink on heat transfer performance using water based graphene nanoplatelets nanofluids. *Int. J. Heat Mass Transf.* **2017**, *106*, 465–472. [\[CrossRef\]](#)
84. Akhavan-Zanjani, H.; Saffar-Avval, M.; Mansourkiaei, M.; Sharif, F.; Ahadi, M. Experimental investigation of laminar forced convective heat transfer of graphene-water nanofluid inside a circular tube. *Int. J. Therm. Sci.* **2016**, *100*, 316–323. [\[CrossRef\]](#)
85. Agromayor, R.; Cabaleiro, D.; Pardinas, A.A.; Vallejo, J.P.; Fernandez-Seara, J.; Lugo, L. Heat transfer performance of functionalized graphene nanoplatelet aqueous nanofluids. *Materials* **2016**, *9*, 455. [\[CrossRef\]](#) [\[PubMed\]](#)
86. Nazari, M.A.; Ahmadi, M.H.; Sadeghzadeh, M.; Shafii, M.B.; Goodarzi, M. A review on application of nanofluid in various types of heat pipes. *J. Cent. S. Univ.* **2019**, *26*, 1021–1041. [\[CrossRef\]](#)
87. Ganvir, R.B.; Walke, P.V.; Kriplani, V.M. Heat transfer characteristics in nanofluid—A review. *Renew. Sustain. Energy Rev.* **2017**, *75*, 451–460. [\[CrossRef\]](#)
88. Sharma, A.K.; Tiwari, A.K.; Dixit, A.R. Progress of nanofluid application in machining: A Review. *Mater. Manuf. Process.* **2015**, *30*, 813–828. [\[CrossRef\]](#)
89. Suleimanov, B.A.; Ismailov, F.S.; Veliyev, E.F. Nanofluid for enhanced oil recovery. *J. Pet. Sci. Eng.* **2011**, *78*, 431–437. [\[CrossRef\]](#)
90. Le Ba, T.; Mahian, O.; Wongwises, S.; Szilágyi, I.M. Review on the recent progress in the preparation and stability of graphene-based nanofluids. *J. Therm. Anal. Calorim.* **2020**, *142*, 1145–1172. [\[CrossRef\]](#)
91. Pavía, M.; Alajami, K.; Estellé, P.; Desforges, A.; Vigolo, B. A critical review on thermal conductivity enhancement of graphene-based nanofluids. *Adv. Colloid Interface Sci.* **2021**, *294*, 102452. [\[CrossRef\]](#)
92. Mehrali, M.; Sadeghinezhad, E.; Latibari, S.T.; Kazi, S.N.; Mehrali, M.; Zubir, M.N.B.M.; Metselaar, H.S.C. Investigation of thermal conductivity and rheological properties of nanofluids containing graphene nanoplatelets. *Nanoscale Res. Lett.* **2014**, *9*, 15. [\[CrossRef\]](#)
93. Sarsam, W.S.; Amiri, A.; Zubir, M.N.M.; Yarmand, H.; Kazi, S.N.; Badarudin, A. Stability and thermophysical properties of water-based nanofluids containing triethanolamine-treated graphene nanoplatelets with different specific surface areas. *Colloids Surfaces A Physicochem. Eng. Asp.* **2016**, *500*, 17–31. [\[CrossRef\]](#)
94. Yarmand, H.; Gharehkhani, S.; Shirazi, S.F.S.; Amiri, A.; Alehashem, M.S.; Dahari, M.; Kazi, S.N. Experimental investigation of thermo-physical properties, convective heat transfer and pressure drop of functionalized graphene nanoplatelets aqueous nanofluid in a square heated pipe. *Energy Convers. Manag.* **2016**, *114*, 38–49. [\[CrossRef\]](#)
95. Khosrojerdi, S.; Vakili, M.; Yahyaei, M.; Kalhor, K. Thermal conductivity modeling of graphene nanoplatelets/deionized water nanofluid by MLP neural network and theoretical modeling using experimental results. *Int. Commun. Heat Mass Transf.* **2016**, *74*, 11–17. [\[CrossRef\]](#)
96. Tahani, M.; Vakili, M.; Khosrojerdi, S. Experimental evaluation and ANN modeling of thermal conductivity of graphene oxide nanoplatelets/deionized water nanofluid. *Int. Commun. Heat Mass Transf.* **2016**, *76*, 358–365. [\[CrossRef\]](#)
97. Bihun, R.I.; Stasyuk, Z.V.; Balitskii, O.A. Crossover from quantum to classical electron transport in ultrathin metal films. *Physica B Condensed Matter* **2016**, *487*, 73–77. [\[CrossRef\]](#)
98. Aksimentyeva, O.I.; Demchenko, P.Y.; Savchyn, V.P.; Balitskii, O.A. The chemical exfoliation phenomena in layered GaSe-polyaniline composite. *Nanoscale Res. Lett.* **2013**, *8*, 1–5. [\[CrossRef\]](#) [\[PubMed\]](#)
99. Sasmito, A.P.; Kurnia, J.C.; Mujumdar, A.S. Numerical evaluation of laminar heat transfer enhancement in nanofluid flow in coiled square tubes. *Nanoscale Res. Lett.* **2011**, *6*, 376. [\[CrossRef\]](#) [\[PubMed\]](#)
100. Choi, S.U.S.; Eastman, J.A. Enhancing thermal conductivity of fluids with nanoparticles. *Am. Soc. Mech. Eng.* **1995**, *231*, 99–106.
101. Teng, T.P.; Hung, Y.H.; Teng, T.C.; Mo, H.E.; Hsu, H.G. The effect of alumina/water nanofluid particle size on thermal conductivity. *Appl. Therm. Eng.* **2010**, *30*, 2213–2218. [\[CrossRef\]](#)

102. Nallusamy, S. Characterization of Al₂O₃/water nanofluid through shell and tube heat exchangers over parallel and counter flow. *J. Nano Res.* **2017**, *45*, 155–163. [[CrossRef](#)]
103. Haddad, Z.; Abid, C.; Oztop, F.H.; Mataoui, A. A review on how the researchers prepare their nanofluids. *Int. J. Therm. Sci.* **2014**, *76*, 168–189. [[CrossRef](#)]
104. Sahin, B.; Gültekin, G.G.; Manay, E. Experimental investigation of heat transfer and pressure drop characteristics of Al₂O₃–water nanofluid. *Exp. Therm. Fluid Sci.* **2013**, *50*, 21–28. [[CrossRef](#)]
105. Balyts'kyi, O.O. Elastic characteristics of laminated gallium and indium chalcogenides. *Mater. Sci.* **2004**, *40*, 706–709. [[CrossRef](#)]
106. Chandrasekar, M.; Suresh, S.; Bose, A.C. Experimental investigations and theoretical determination of thermal conductivity and viscosity of Al₂O₃/water nanofluid. *Exp. Therm. Fluid Sci.* **2010**, *34*, 210–216. [[CrossRef](#)]
107. Roy, G.; Nguyen, C.T.; Lajoie, P.R. Numerical investigation of laminar flow and heat transfer in a radial flow cooling system with the use of nanofluids. *Superlattices Microstruct.* **2004**, *35*, 497–511. [[CrossRef](#)]
108. Maiäga, S.; Nguyen, C.T.; Galanis, N. Heat transfer behaviours of nanofluids in a uniformly heated tube. *Superlattices Microstruct.* **2004**, *35*, 543–577. [[CrossRef](#)]
109. Anoop, K.B.; Sundararajan, T.; Das, K.S. Effect of particle size on the convective heat transfer in nanofluid in the developing region. *Int. J. Heat Mass Tran.* **2009**, *52*, 2189–2195. [[CrossRef](#)]
110. Timofeeva, E.V.; Yu, W.; France, M.D. Base fluid and temperature effects on the heat transfer characteristics of SiC in ethylene glycol/H₂O and H₂O nanofluids. *J. Appl. Phys.* **2011**, *109*, 014914. [[CrossRef](#)]
111. Esfe, M.H.; Saedodin, S. Turbulent forced convection heat transfer and thermophysical properties of MgO–water nanofluid with consideration of different nanoparticles diameter, an empirical study. *J. Therm. Anal. Calorim.* **2015**, *119*, 1205–1213. [[CrossRef](#)]
112. Arani, A.; Amani, J. Experimental investigation of diameter effect on heat transfer performance and pressure drop of TiO₂–water nanofluid. *Exp. Therm. Fluid Sci.* **2013**, *44*, 520–533. [[CrossRef](#)]
113. Dawood, H.K.; Mohammed, H.A.; Sidik, N.A.C. Heat transfer augmentation in concentric elliptic annular by ethylene glycol based nanofluids. *Int. Commun. Heat Mass Transf.* **2017**, *82*, 29–39. [[CrossRef](#)]
114. Elsebay, M.; Elbadawy, I.; Shedid, M.H. Numerical resizing study of Al₂O₃ and CuO nanofluids in the flat tubes of a radiator. *Appl. Math. Model.* **2016**, *40*, 6437–6450. [[CrossRef](#)]
115. Farajollahi, B.; Etemad, S.G.; Hojjat, M. Heat transfer of nanofluids in a shell and tube heat exchanger. *Int. J. Heat Mass Tran.* **2010**, *53*, 12–17. [[CrossRef](#)]
116. Hayder, A.D.; Sinan, A.A.; Miqdam, T.C. Combustion analysis and performance characteristics of compression ignition engines with diesel fuel supplemented with nano-TiO₂ and nano-Al₂O₃. *Case Stud. Therm. Eng.* **2020**, *20*, 100651.
117. Nassir, A.K.; Shahad, H.A.K. Experimental study of a diesel engine performance fueled with different types of nano-fuel. *J. Univ. Babylon Eng. Sci.* **2018**, *26*, 36–57. [[CrossRef](#)]
118. Balyts'kyi, O.I.; Kostyuk, I.F. Strength of welded joints of Cr-Mn steels with elevated content of nitrogen in hydrogen-containing media. *Mater. Sci.* **2009**, *41*, 97–107. [[CrossRef](#)]
119. Chaichan, M.T. Performance and emissions characteristics of CIE using hydrogen, biodiesel, and massive EGR. *Int. J. Hydrogen Energy* **2018**, *43*, 5415–5435. [[CrossRef](#)]
120. Soudagar, M.E.M.; Ghazali, N.N.; Kalam, M.A.; Badruddin, I.A.; Banapurmath, N.R.; Khan, T.M.; Bashir, Y.M.N.; Akram, N.; Farade, R.; Afzal, A. The effects of graphene oxide nanoparticle additive stably dispersed in dairy scum oil biodiesel-diesel fuel blend on CI engine: Performance, emission and combustion characteristics. *Fuel* **2019**, *257*, 116015. [[CrossRef](#)]
121. Yaşar, A.; Keskin, A.; Yıldızhan, Ş.; Uludamar, E. Emission and vibration analysis of diesel engine fueled diesel fuel containing metallic based nanoparticles. *Fuel* **2019**, *239*, 1224–1230. [[CrossRef](#)]
122. D'Silva, R.; Binu, K.G.; Bhat, T. Performance and Emission characteristics of a CI Engine fueled with diesel and TiO₂ nanoparticles as fuel additive. *Mater. Today Proc.* **2015**, *2*, 3728–3735. [[CrossRef](#)]
123. Karthikeyan, S.; Elango, A.; Prathima, A. Performance and emission study on zinc oxide nano particles addition with pomoplion stearin wax biodiesel of CI engine. *J. Sci. Ind. Res.* **2014**, *73*, 187–190.
124. Tyagi, H.; Phelan, P.E.; Prasher, R.; Peck, R.; Lee, T.; Pacheco, J.R.; Arentzen, P. Increased hotplate ignition probability for nanoparticle-laden diesel fuel. *Nano Lett.* **2008**, *8*, 1410–1416. [[CrossRef](#)]
125. Vellaiyana, S.; Subbiah, A.; Chockalingam, P. Multi-response optimization to improve the performance and emissions level of a diesel engine fueled with ZnO incorporated water emulsified soybean biodiesel/diesel fuel blends. *Fuel* **2019**, *237*, 1013–1020. [[CrossRef](#)]
126. Srinidhia, C.; Madhusudhan, A.; Channapattana, S.V. Effect of NiO nanoparticles on performance and emission characteristics at various injection timings using biodiesel-diesel blends. *Fuel* **2019**, *235*, 185–193. [[CrossRef](#)]
127. Saxena, V.; Kumar, N.; Saxena, V.K. A comprehensive review on combustion and stability aspects of metal nanoparticles and its additive effect on diesel and biodiesel fueled CI engine. *Renew. Sustain. Energy Rev.* **2017**, *70*, 563–588. [[CrossRef](#)]
128. Soudagar, M.E.M.; Nik-Ghazali, N.N.; Kalam, M.A.; Badruddin, I.A.; Banapurmath, N.R.; Akram, N. The effect of nano-additives in diesel-biodiesel fuel blends: A comprehensive review on stability, engine performance and emission characteristics. *Energy Convers. Manag.* **2018**, *178*, 146–177. [[CrossRef](#)]
129. Hamadi, A.S.; Dhahad, H.A.; Khidhir, A.G. An experimental investigation of Impact of ZrO₂ nanoparticles in DI engine performance. *Kirkuk Univ. J. Sci. Stud. (KUJSS)* **2019**, *14*, 67–85. [[CrossRef](#)]

130. Ekaab, N.S.; Hamza, N.H.; Chaichan, M.T. Performance and emitted pollutants assessment of diesel engine fueled with Biokerosene. *Case Stud. Therm. Eng.* **2019**, *13*, 100381. [[CrossRef](#)]
131. Chaichan, M.T.; Kadhum, A.H.; Al-Amiery, A.A. Novel technique for enhancement of diesel fuel: Impact of aqueous alumina nano-fluid on engine's performance and emissions. *Case Stud. Therm. Eng.* **2017**, *10*, 611–620. [[CrossRef](#)]
132. Chaichan, M.T. Combustion and emission characteristics of E85 and diesel blend in conventional diesel engine operating in PPCI mode. *Therm. Sci. Eng. Progr.* **2018**, *7*, 45–53. [[CrossRef](#)]
133. Alam, M.A.; Samad, U.A.; Khan, R.; Alam, M.; Al-Zahrani, S.M. Anti-corrosive performance of epoxy coatings containing various nano-particles for splash zone applications. *Korean J. Chem. Eng.* **2017**, *34*, 2301–2310. [[CrossRef](#)]
134. Ganesh, V.; Shumaila, J.; Al-Mdallal, Q.M.; Kalaivanan, R.; Chamkha, A.J. Numerical study of heat generating γ Al₂O₃-H₂O nanofluid inside a square cavity with multiple obstacles of different shapes. *Heliyon* **2020**, *6*, e05752. [[CrossRef](#)] [[PubMed](#)]
135. Moghaieb, H.S.; Abdel-Hamid, H.M.; Shedid, M.H.; Helali, A.B. Engine cooling using Al₂O₃/water nanofluids. *Appl. Therm. Eng.* **2017**, *115*, 152–159. [[CrossRef](#)]
136. Radwan, M.S.; Saleh, H.E.; Attai, Y.A.; Elsherbiny, M.S. On heat transfer enhancement in diesel engine cylinder head using γ -Al₂O₃/water nanofluid with different nanoparticle sizes. *Adv. Mech. Eng.* **2020**, *12*, 16878. [[CrossRef](#)]
137. Nowrouzi, I.; Manshad, A.K.; Mohammadi, A.H. Effects of TiO₂, MgO and γ -Al₂O₃ nano-particles on wettability alteration and oil production under carbonated nano-fluid imbibition in carbonate oil reservoirs. *Fuel* **2020**, *259*, 116110. [[CrossRef](#)]
138. Abdul-Aziz, M.; Azza, H.; Ali, H.; Elkhatib, H.; Othman, S. Effect of operating parameters on the transient behavior of gravity-assisted heat-pipe using radio-chemically prepared γ Al₂O₃ nano-fluid. *Adv. Powder Technol.* **2016**, *27*, 1651–1662. [[CrossRef](#)]
139. Bayomy, A.M.; Saghir, M.Z. Experimental study of using γ -Al₂O₃-water nanofluid flow through aluminium foam heat sink: Comparison with numerical approach. *Int. J. Heat Mass Tran.* **2017**, *107*, 181–203. [[CrossRef](#)]
140. Vishnu Ganesh, N.; Abdul Hakeem, A.K.; Ganga, B. A comparative theoretical study on Al₂O₃ and γ -Al₂O₃ nanoparticles with different base fluids over a stretching sheet. *Adv. Powder Technol.* **2016**, *27*, 436–441. [[CrossRef](#)]
141. Rashidi, M.M.; Vishnu Ganesh, N.; Abdul Hakeem, A.K.; Ganga, B.; Lorenzini, G. Influences of an effective Prandtl number model on nano boundary layer flow of γ Al₂O₃-H₂O and γ Al₂O₃-C₂H₆O₂ over a vertical stretching sheet. *Int. J. Heat Mass Tran.* **2016**, *98*, 616–623. [[CrossRef](#)]
142. Vishnu, G.N.; Kameswaran, P.K.; Al-Mdallal, Q.M.; Hakeem, A.K.; Ganga, B. Non-linear thermal radiative Marangoni boundary layer flow of gamma Al₂O₃ nanofluids past a stretching sheet. *J. Nanofluids* **2018**, *7*, 944–950.
143. Vishnu Ganesh, N.; Chamkha, A.J.; Al-Mdallal, Q.M.; Kameswaran, P.K. Magneto-Marangoni nano-boundary layer flow of water and ethylene glycol based γ Al₂O₃ nanofluids with non-linear thermal radiation effects. *Case Stud. Thermal Eng.* **2018**, *12*, 340–348. [[CrossRef](#)]
144. Mahmoudi, A.I.; Mejri, M.A.; Abbassi, A.; Omri, A. Analysis of MHD natural convection in a nanofluid-filled open cavity with non uniform boundary condition in the presence of uniform heat generation/absorption. *Powder Technol.* **2015**, *269*, 275–289. [[CrossRef](#)]
145. Rashad, A.M.; Rashidi, M.M.; Lorenzini, G.; Ahmed, S.E.; Aly, A.M. Magnetic field and internal heat generation effects on the free convection in a rectangular cavity filled with a porous medium saturated with Cu-water nanofluid. *Int. J. Heat Mass Tran.* **2017**, *104*, 878–889. [[CrossRef](#)]
146. Selimefendigil, F.; Öztop, H.F. Mixed convection in a partially heated triangular cavity filled with nanofluid having a partially flexible wall and internal heat generation. *J. Taiwan Inst. Chem. Eng.* **2017**, *70*, 168–178. [[CrossRef](#)]
147. Rashad, A.M.; Chamkha, A.J.; Ismael, M.A.; Salah, T. Magnetohydrodynamics natural convection in a triangular cavity filled with a Cu-Al₂O₃/water hybrid nanofluid with localized heating from below and internal heat generation. *J. Heat Tran.* **2018**, *140*, 072502. [[CrossRef](#)]
148. Benos, L.; Sarris, I.E. Analytical study of the magnetohydrodynamic natural convection of a nanofluid filled horizontal shallow cavity with internal heat generation. *Int. J. Heat Mass Tran.* **2019**, *130*, 862–873. [[CrossRef](#)]
149. Armaghani, T.; Chamkha, A.; Rashad, A.M.; Mansour, M.A. Inclined magneto: Convection, internal heat, and entropy generation of nanofluid in an I-shaped cavity saturated with porous media. *J. Therm. Anal. Calorim.* **2020**, *142*, 2273–2285. [[CrossRef](#)]
150. Selimefendigil, F.; Öztop, H.F. Natural convection and entropy generation of nanofluid filled cavity having different shaped obstacles under the influence of magnetic field and internal heat generation. *J. Taiwan Inst. Chem. Eng.* **2015**, *56*, 42–56. [[CrossRef](#)]
151. Sheikholeslami, M. Influence of magnetic field on Al₂O₃-H₂O nanofluid forced convection heat transfer in a porous lid driven cavity with hot sphere obstacle by means of LBM. *J. Mol. Liq.* **2018**, *263*, 472–488. [[CrossRef](#)]
152. Hamid, M.; Khan, Z.H.; Khan, W.A.; Haq, R.U. Natural convection of water-based carbon nanotubes in a partially heated rectangular fin-shaped cavity with an inner cylindrical obstacle. *Phys. Fluids* **2019**, *31*, 103607. [[CrossRef](#)]
153. Alkanhal, T.A.; Sheikholeslami, M.; Usman, M.; Haq, R.U.; Shafee, A.; Al-Ahmadi, A.S.; Tlili, I. Thermal management of MHD nanofluid within the porous medium enclosed in a wavy shaped cavity with square obstacle in the presence of radiation heat source. *Int. J. Heat Mass Tran.* **2019**, *139*, 87–94. [[CrossRef](#)]
154. Usman, M.; Khan, Z.H.; Liu, M.B. MHD natural convection and thermal control inside a cavity with obstacles under the radiation effects. *Phys. Stat. Mech. Appl.* **2019**, *535*, 122443. [[CrossRef](#)]
155. Selimefendigil, F.; Öztop, H.F. Control of natural convection in a CNT-water nanofluid filled 3D cavity by using an inner T-shaped obstacle and thermoelectric cooler. *Int. J. Mech. Sci.* **2020**, *169*, 105104. [[CrossRef](#)]

156. Azizul, F.M.; Alsabery, A.I.; Hashim, I. Heatlines visualisation of mixed convection flow in a wavy heated cavity filled with nanofluids and having an inner solid block. *Int. J. Mech. Sci.* **2020**, *175*, 105529. [[CrossRef](#)]
157. Rehman, K.U.; Al-Mdallal, Q.M.; Tlili, I.; Malik, M.Y. Impact of heated triangular ribs on hydrodynamic forces in a rectangular domain with heated elliptic cylinder: Finite element analysis. *Int. Commun. Heat Mass Tran.* **2020**, *112*, 104501. [[CrossRef](#)]
158. Rehman, K.U.; Al-Mdallal, Q.M.; Qaiser, A.; Malik, M.Y.; Ahmed, M.N. Finite element e amination of hydrodynamic forces in grooved channel having two partially heated circular cylinders. *Case Stud. Thermal Eng.* **2020**, *18*, 100600. [[CrossRef](#)]
159. Rehman, K.U.; Al-Mdallal, Q.M. On partially heated circular obstacle in a channel having heated rectangular ribs: Finite element outcomes. *Case Stud. Thermal Eng.* **2020**, *18*, 100597. [[CrossRef](#)]
160. Karbalaei, A.; Cho, H.J. Passive mixing rate of trapped squeezed nanodroplets—A time scale analysis. *Exp. Comput. Multiph. Flow* **2020**, *2*, 135–141. [[CrossRef](#)]
161. Vierecki, F.; Schleicher, E.; Schuster, C.; Lippmann, W.; Hurtado, A. Experimental and theoretical investigation of the boiling heat transfer in a low-pressure natural circulation system. *Exp. Comput. Multiph. Flow* **2019**, *1*, 286–299. [[CrossRef](#)]
162. Behzad, M.; Botlani Esfahani, S.; Sajadi, M.; Baleanu, D. The effect of sedimentation phenomenon of the additives silver nano particles on water pool boiling heat transfer coefficient: A comprehensive experimental study. *J. Mol. Liq.* **2021**, *345*, 117891.
163. Choi, E.S.; Brooks, J.S.; Eaton, D.L.; Al-Haik, M.S.; Hussiani, M.Y.; Garmestani, H.; Li, D.; Dahmen, K. Enhancement of thermal and ecktrical properties of carbon nanotube polymer composites by magnetic field processing. *J. Appl. Phys.* **2003**, *94*, 6034–6039. [[CrossRef](#)]
164. Chien-Chih, L.; Jenn-Gwo, H. Performance enhancement of metal-oxidesemiconductor tunneling temperature sensors with nanoscale oxides by employing ultrathin Al₂O₃ high-k dielectrics. *Nanoscale* **2013**, *5*, 8090.
165. Heris, S.Z.; Etemad, S.G.; Esfahany, M.N. Experimental investigation of oxide nanofluids laminar flow convective heat transfer. *Int. Commun. Heat Mass* **2006**, *33*, 529–535. [[CrossRef](#)]
166. Peng-Cheng, P.; Chen Xiaolong, C.; LiuJames, L.; Hedrick Zhuang, H.; Shunzhi, X.; Qing-Yuan, W.; Lin-Mark, C.; Hersam Vinayak, P.; Chad, D.; Mirkin, A. Polyelemental nanoparticle libraries. *Science* **2016**, *352*, 1565–1569.
167. Alaraji, K.M.; Hachim, D.M.; Almoussawi, M.A. Nano-Fluids as a Coolant for Automotive Engine Radiators: Review Study. *J. Innov. Mech. Sustain. Energy Eng. (FJIMSE)* **2021**, *1*, 28–50.
168. Zhao, N.; Li, S.; Yang, J. A review on nanofluids: Data-driven modeling of thermal physical properties and the application in automotive radiator. *Renew. Sustain. Energy Rev.* **2016**, *66*, 596–616. [[CrossRef](#)]
169. Angadi, V.M.; Nagaraj, R.; Hebbal, O.D. CFD Analysis of heat transfer enhancement of a car radiator using nanofluid as a coolant. *Int. J. Eng. Res. Technol.* **2014**, *3*, 1058–1063.
170. Said, Z. Enhancing the performance of automotive radiators using nanofluids. *Renew. Sustain. Energy Rev.* **2019**, *112*, 183–194. [[CrossRef](#)]
171. Tafakhori, M.; Kalantari, D.; Biparva, P.; Peyghambarzadeh, S.M. Assessment of Fe₃O₄–water nanofluid for enhancing laminar convective heat transfer in a car radiator. *J. Therm. Anal. Calorim.* **2020**, *146*, 841–853. [[CrossRef](#)]
172. Ebrahimi, M.; Farhadi, M.; Sedighi, K.; Akbarzade, S. Experimental investigation of force convection heat transfer in a car radiator filled with SiO₂-water nanofluid. *Int. J. Eng. Trans. B Appl.* **2014**, *27*, 333–340. [[CrossRef](#)]
173. Nieh, H.M.; Teng, T.P.; Yu, C.C. Enhanced heat dissipation of a radiator using oxide nano coolant. *Int. J. Therm. Sci.* **2014**, *77*, 252–261. [[CrossRef](#)]
174. Hussein, A.M.; Bakar, R.A.; Kadrigama, K. Study of forced convection nanofluid heat transfer in the automotive cooling system. *Case Stud. Therm. Eng.* **2014**, *2*, 50–61. [[CrossRef](#)]
175. Balyts'kyi, O.I.; Ivaskevich, L.M.; Mochylskii, V.M. Mechanical properties of martensitic steels in gaseous hydrogen. *Strength Mater.* **2012**, *44*, 64–73. [[CrossRef](#)]
176. Tkachev, V.I.; Levina, I.M.; Ivas'kevych, L.M. Distinctive features of hydrogen degradation of heat-resistant alloys based on nickel. *Mater. Sci.* **1997**, *33*, 524–531. [[CrossRef](#)]
177. Peyghambarzadeh, S.M.; Hashemabadi, S.H.; Naraki, M.; Vermahmoudi, Y. Experimental study of overall heat transfer coefficient in the application of dilute nanofluids in the car radiator. *Appl. Therm. Eng.* **2013**, *52*, 8–16. [[CrossRef](#)]
178. Heris, S.Z.; Shokrgozar, M.; Poorpharhang, S.; Shanbedi, M.; Noie, S.H. Experimental study of heat transfer of a car radiator with CuO/Ethylene Glycol-water as a coolant. *J. Dispers. Sci. Technol.* **2014**, *35*, 677–684. [[CrossRef](#)]
179. Ali, H.M.; Azhar, M.D.; Saleem, M.; Saeed, Q.S.; Saieed, A. Heat transfer enhancement of car radiator using aqua-based magnesium oxide nanofluids. *Therm. Sci.* **2015**, *19*, 2039–2048. [[CrossRef](#)]
180. Teng, T.P.; Yu, C.C. Heat dissipation performance of MWCNTs nano-coolant for vehicle. *Exp. Therm. Fluid Sci.* **2013**, *49*, 22–30. [[CrossRef](#)]
181. Hussein, A.M.; Bakar, R.A.; Kadrigama, K.; Sharma, K.V. Heat transfer augmentation of a car radiator using nanofluids. *Heat Mass Transf. Stoffuebertragung* **2014**, *50*, 1553–1561. [[CrossRef](#)]
182. Che Sidik, N.A.C.; Yazid, M.N.A.W.M.; Mamat, R. A review on the application of nanofluids in vehicle engine cooling system. *Int. Commun. Heat Mass Transf.* **2015**, *68*, 85–90. [[CrossRef](#)]
183. Mohammadreza, A.; Ommi, F. Using nanofluid for heat transfer enhancement in engine cooling process. *J. Nano Energy Power Res.* **2013**, *2*, 132–134.
184. Moita, A.; Moreira, A.; Pereira, J. Nanofluids for the next generation thermal management of electronics: A Review. *Symmetry* **2021**, *13*, 1362. [[CrossRef](#)]